Electron Backscattering Diffraction Investigation of Focused Ion Beam Surfaces

T.L. MATTESON,[1] S.W. SCHWARZ,[1] E.C. HOUGE,[1,2] B.W. KEMPSHALL,[1] and L.A. GIANNUZZI[1]

1.—Mechanical, Materials & Aerospace Engineering, University of Central Florida, Orlando, FL 32816. 2.—Cirent Semiconductor/Agere Systems, 9333 S. John Young Pkwy., Orlando, FL 32819

A focused ion beam (FIB) instrument has been used to mill surfaces in single-crystal Si and single-crystal Cu for subsequent electron backscattering diffraction (EBSD) analysis. The FIB cuts were performed using a 30 keV and a 5 keV Ga^+ ion beam at a stage tilt of 20° to provide a readily obtainable 70° surface for direct EBSD investigation in a scanning electron microscope (SEM). The quality of the patterns is related to the amount of FIB damage induced in the Cu and Si. These or similar methods should be directly transferable to a FIB/SEM dual beam instrument equipped with an EBSD detector.

Key words: FIB, EBSD, EBSP, Cu, Si, FIB damage, amorphous, TRIM, image quality, dual beam

INTRODUCTION

Background on EBSD

The primary strength of electron backscattering diffraction (EBSD) techniques in a scanning electron microscope (SEM) is the ability to study both the morphology (via SEM) and the crystallographic relationships of polycrystalline phases (via EBSD) simultaneously. When a focused electron beam impinges on a crystal with an inclined surface of approximately 70°, a reflection Kikuchi pattern of intersecting bands may be obtained as a result of diffraction of backscattered electrons. Indexable electron backscattered diffraction patterns (EBSPs) may be obtained from a ~22-nm region using an SEM equipped with a field emission source.[1]

The quality of the EBSP decreases with increased defect density in the sample. The image quality (IQ) depends on the material, its surface quality, the technique and parameters used to index the patterns, crystallographic orientation, as well as other factors. Elements with higher atomic numbers generally produce stronger patterns due to increased backscattering. A rough surface will also produce variations in IQ due to the deviation in the surface plane from the ideal 70° tilt for diffraction. The surface quality of the crystal lattice within the diffracting volume may affect the quality of the EBSP. Any lattice strain within the diffraction volume will produce lower quality diffraction patterns. Since the IQ also depends on the crystallographic orientation of a given material, it cannot be used to distinguish small strain differences from grain to grain. However, a determination of the IQ may be used to yield a qualitative description of the strain distribution in a polycrystalline microstructure.[2]

Because the IQ parameter is also a function of the indexing method, any parameters that effect the operation of the indexing method would effect the resulting IQ parameter calculation. In order to obtain a crystal's orientation from a diffraction pattern, the pattern must be indexed. Using the Hough transform method, the IQ parameter is the average value of the heights of the most prominent detected peaks in the Hough transform.[3] Thus, in general, a larger IQ indicates a better pattern.

There is still debate as to the magnitude of the surface depth from which the EBSP originates. Since EBSP bands are sharp and discrete, it is assumed that the backscattered electrons that contribute to the pattern lose no more than ~100 eV.[4] Therefore, EBSPs are formed from the near surface regions of a sample. The surface depth of the backscattered electrons having this energy loss may be determined using Monte Carlo simulations. The depth is a function of the extinction distance for electrons, and, therefore, it varies for different re-

(Received July 17, 2001; accepted September 14, 2001)

flections. Calculations show that the contrast of the channeling drops rapidly for a thickness greater than two extinction distances (e.g., ~100 nm).[5] For EBSPs obtained from a field emission source, patterns have been obtained from volumes 20 nm × 80 nm × 10 nm.[6] However, when considering possible surface damage, the magnitude of the interaction volume that is of most interest is the amount of material below the damage (or other) layer thickness required to produce a pattern that is sufficient to overcome any absorption during backscattering through the same layer. Thus, a study on focused ion beam damage on the quality of EBSPs has been initiated.

Background on FIB and Ion Beam/Material Interactions

The focused ion beam (FIB) instrument has come into the forefront of analytical instruments for device and mask repair in the semiconductor market, micro- and nanomachining, and as a specimen preparation tool spanning the physical and biological sciences. The FIB is now widely used for specimen preparation for scanning electron microscopy and transmission electron microscopy (TEM) analyses, and it is also being pursued as a general specimen preparation method for analysis by, e.g., Auger electron spectroscopy and secondary ion mass spectrometry (SIMS).[7] In an FIB instrument, ions (typically Ga^+) obtained from a liquid metal ion source are accelerated down a column at energies up to ~50 keV. Beam sizes in FIB instruments on the order of 5–7 nm may be achieved. The primary ion beam interaction with the target results in the emission of secondary ions and secondary electrons, either of which may be collected to form an image. Large regions of material (e.g., 500 μm^3) can be removed at high beam currents in just a couple of minutes, while lower beam currents (smaller beam diameters) are used to remove smaller amounts of material within the same time frame (e.g., ~5 μm^3).

Specimen preparation by FIB uses the process of ion bombardment to selectively remove material. Atoms that are displaced from their equilibrium positions by the impingement of energetic ions generate a collision cascade within the target material. Sputtering occurs if sufficient momentum is transferred to a surface atom. The nature of the cascade depends on the incident ion energy and the ratio of the target (M2) to ion mass (M1). If M1 << M2, then single knock-on occurs. That is, the target atoms do not receive enough energy to generate a cascade and sputtering is minimal. The FIB instrument generally operates in a linear cascade regime where the ion energies are moderate and M1 ~ M2. Thus, recoil atoms receive enough energy to generate a cascade. In this regime, the number of moving atoms is small with respect to the total number of atoms contained within the collision volume.[8]

One consequence of ion implantation can be the development of a surface amorphous phase. The amorphous phase induced in crystalline materials by ion bombardment is typically metastable, and its formation depends on unit cell size, complexity of chemical ordering, and the width of an intermetallic phase field.[9] The restoration of the collision cascade induced disorder requires correlated and cooperative motion of alloying atoms. The more complex the material unit cell, the larger the amorphous layer will be. Likewise, smaller unit-celled materials are difficult to amorphize. Additionally, alloys or materials with a broad phase field will remain crystalline, because the atomic packing arrangement is less stringent than line compounds or stochiometric intermetallics.

FIB Damage in Si

The amorphization of Si as a result of FIB milling is well known. For any given material, the amorphization layer thickness would depend on the incident ion species, incident angle, and incident ion energy. For Si, amorphization FIB damage at high (i.e., glancing) incident angles has typically been reported in the ~10–30 nm range.[10,11] In a previous report from our lab, we have shown a cross section of Si from a FIB milled cut specific to FEI instruments known as the "clean up cut" (CUC).[12] In the CUC, the beam is scanned one line at a time toward the region of interest. Because each line overlaps the previously milled surface as it progresses toward the region of interest, sputtering occurs on a side wall, which has an overall effect of creating a deeper cut for each subsequent line scan. In addition, as the beam progresses forward, sputtered material may redeposit onto the previously milled surface. A CUC in Si was milled using a beam current of 1000 pA. The sample was then removed from the FIB, sputter coated with Au-Pd, and then placed back into the FIB where the CUC was filled by depositing with Pt. A cross-sectional TEM specimen of the CUC was prepared by the lift out technique.[13,14] A TEM cross-sectional image of a portion of the CUC in Si at 1000 pA is shown in Fig. 1a. The single-crystal Si is denoted by the ubiquitous [011] selected area diffraction pattern (SADP). Note that the beam scan positions may be observed and the beam size may be estimated at ~100 nm. The redeposited Si is readily observable via a change in contrast in the image, and is also indicated by the nanocrystalline (nearly amorphous) SADP pattern shown in the inset. The amorphization FIB damage is evident between the single-crystal Si and the nanocrystalline redeposited Si along the side-wall cut and the outline of the beam position.

FIB Damage in Cu

Interest in the FIB preparation of Cu has increased due to its increased use for metallization layers in silicon-based integrated circuits. Thus, to ascertain the FIB damage in Cu, a CUC was milled at 1000 pA into (001) Cu. The Cu was cross sectioned and prepared for TEM analysis in the

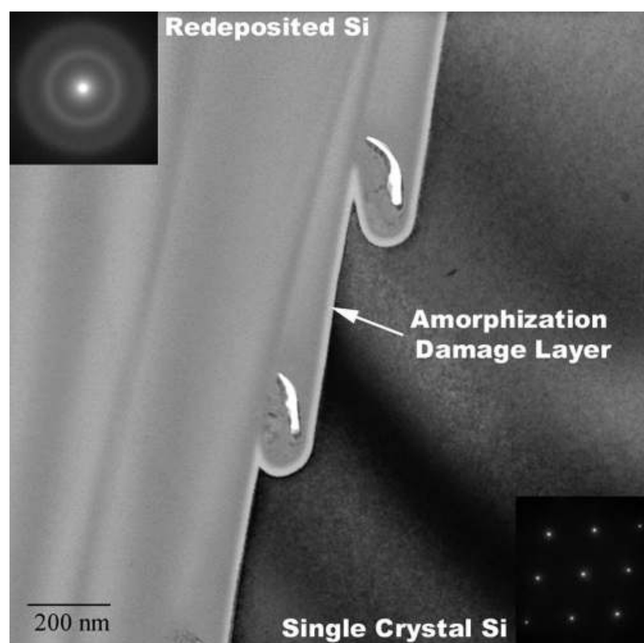

a

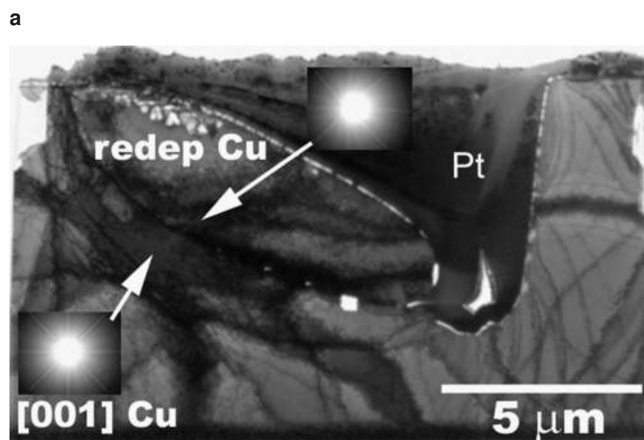

b

Fig. 1. (a) A cross-sectional TEM image of a CUC in Si. (b) A cross-sectional TEM image of a CUC in Cu.

same manner described above for the Si CUC. The entire cross section of the CUC is shown in the low-magnification TEM image in Fig. 1b. Insets show convergent beam electron diffraction (CBED) patterns obtained from the Cu substrate and the redeposited Cu region. Note that in Fig. 1(b), the CUC begins on the left side of the image and progresses toward the region of interest to the right. A [001] CBED pattern of the Cu substrate obtained from the region of intersecting bend contours (indicated by the arrow) is shown in the inset. Note that the bend contours are not continuous across the FIB milled region. A near [001] CBED pattern obtained from the redeposited Cu (its position is indicated by the arrow) is also shown in the figure. Hence, the redeposited Cu CBED represents a single crystal. Thus, it appears that the redeposited Cu nucleated (nearly) epitaxially with the underlying Cu substrate. Therefore, Cu does not amorphize when FIB milled with Ga^+. The dark line of contrast outlining the position of the beam scan corresponds to a wall of dislocations. These are likely misfit dislocations that accommodate the slight deviation in orientation (~2°) between the substrate and the redeposited Cu. In addition, these dislocations may also be attributed to a high density of crystalline defects produced in the Cu by the FIB process.

Thus, TEM cross sections of the FIB milled cuts shows that Cu does not amorphize when exposed to a Ga^+ FIB beam, while Si does amorphize when FIB milled with Ga^+. It is presumed that the surface of the Cu defined by the FIB collision cascade contains crystalline defects, although the specific type of defects is not resolvable from the image shown in Fig. 1b. The observed FIB damage differences between Si and Cu are consistent with the theoretical description of the damage described above. This paper will discuss the quality of EBSPs obtained from FIB prepared surfaces of Si and Cu.

EXPERIMENTAL TECHNIQUES

A (001) cleaved piece of silicon wafer and a section of a (001) single-crystal copper were used in this study. The sample sizes were on the order of ~10 mm × 10 mm in dimension. An FEI 200TEM FIB workstation was used to mill surfaces in the Si and Cu samples. Each sample was mounted on a typical sample stud using silver paint such that each sample surface plane was approximately normal to the FIB beam. The FIB was used to mill an initial trench into each sample at a stage tilt of 20°, as shown in Fig. 2a. Once the initial trench was milled, the sidewall of interest was such that the ion beam was approximately parallel to it (e.g., an ~89° ion beam incident angle with respect to the FIB surface). Note that the surface of interest was milled near the edge of the sample to avoid potential shadowing of the diffracted electrons during subsequent EBSD analysis in the SEM. Tilting and FIB milling the sample at a 20° angle created a 70° milled face that was readily observed by EBSP/SEM (Fig. 2b and c).

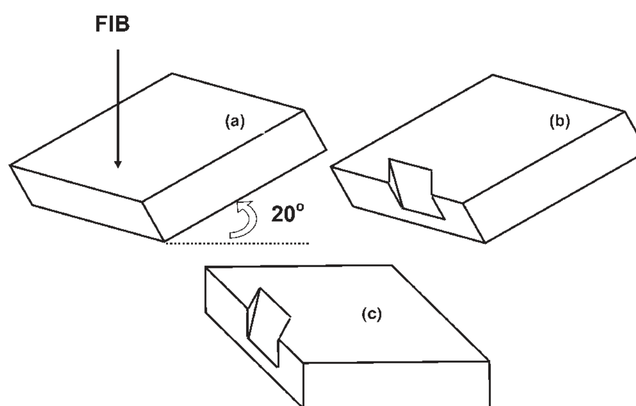

Fig. 2. A schematic diagram of the sample orientation during FIB milling for subsequent EBSP analysis.

All FIB cuts were performed using a beam energy of 30 keV except where noted. To prepare the Si sample for EBSD analysis, the first FIB cut was performed at a stage tilt of 20° using a rectangular trench with dimensions of 20 μm × 5 μm and 20 μm deep at a beam current of 20,000 pA. The second trench cut of the same dimensions as the first cut was performed with a beam current of 500 pA. This second cut slightly overlapped the first. A third rectangular cut having dimensions 20 μm × 0.5 μm and 20 μm deep overlapped the previous at a beam current of 100 pA. A second region of interest was prepared in the same manner as described above. This second region of interest was then tilted back to a stage tilt of 15° (i.e., 5° tilt into the previous cut) and the magnification was increased to include the FIB milled surface of interest in the field of view of the imaging screen. The beam conditions were changed to an energy of 5 keV (with a predefined beam current of 60 pA) and the surface was imaged with the ion beam. That is, the beam was rastered across the region of interest in “imaging” mode rather than in “milling” mode for several minutes in an attempt to reduce the 30 keV milling effects. The Cu sample was prepared in the same manner as the Si sample performed at a beam energy of 30 keV as described above. The EBSPs from the FIB milled surfaces of Si and Cu were obtained with a Hitachi (Japan) 4000 field emission SEM equipped with a TexSEM Laboratories EBSD unit.

RESULTS AND DISCUSSION

An EBSP and corresponding automatically indexed pattern of the FIB surface in Cu obtained using an SEM accelerating voltage of 20 kV is shown in Fig. 3. Note the high quality of the EBSP obtained from this Cu sample. Background subtraction was omitted for this particular pattern because the quality of the pattern did not warrant this procedure. An IQ value of 133 was obtained for the Cu EBSP. The slight deviation in the positions of the indexed pattern may be due to either (1) strain in the Cu lattice due to Ga^+ implantation or (2) incorrect calibration of the EBSD unit. Despite the Ga^+ implantation into the Cu surface, an excellent EBSP was obtained indicating that the ion implantation damage is not sufficient to hinder acquisition of EBSPs for Cu. As such, the use of EBSPs for the analysis of FIB milled Cu was previously confirmed by Ref. 15.

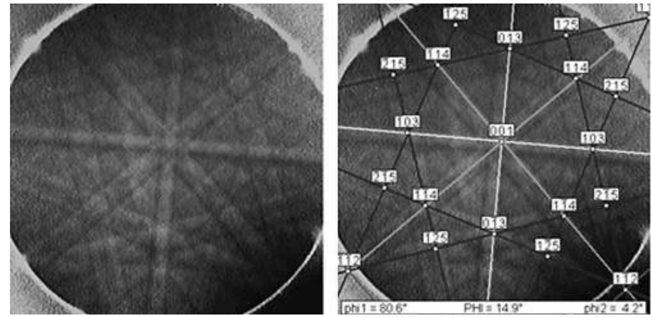

Fig. 3. An EBSP and corresponding indexed pattern obtained from a 30 keV Ga^+ FIB cut in Cu obtained with an SEM accelerating voltage of 20 kV.

The FIB surfaces in Si were analyzed using EBSD methods at an SEM accelerating voltage of 20 kV and 30 kV. In addition, the (001) Si wafer surface was analyzed by the EBSD method at an SEM accelerating voltage of 20 kV to serve as a qualitative reference for the FIB prepared surfaces. A (001) “clean” Si surface was tilted in the SEM to 70° and its EBSP and indexed pattern are shown in Fig. 4. (It is understood that crystal orien-

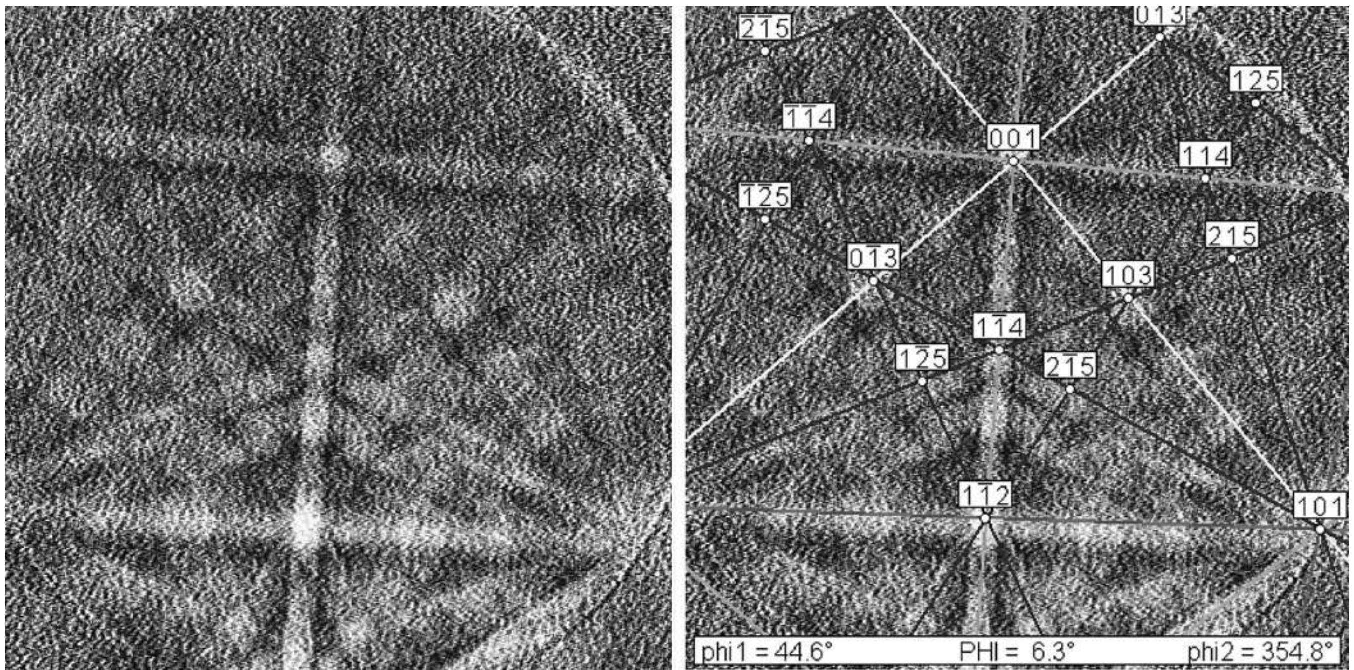

Fig. 4. An EBSP and its indexed pattern obtained from a Si (001) surface.

tation may affect the IQ of the EBSP.) An IQ value of 345 was obtained for the (001) Si surface. The EBSP quality of this surface (Fig. 4) may be compared to the EBSPs from the FIB milled surfaces shown in Fig. 5. Figure 5 shows an EBSP from the 30 keV Si FIB surface observed at 30 kV (IQ = 104), the 5 keV Si FIB surface observed at 30 kV (IQ = 164), the 30 keV Si FIB surface observed at 20 kV (IQ = 67), and the 5 keV Si FIB surface observed at 20 kV (IQ = 89). Note that all images in Figs. 4 and 5 were obtained using background subtraction. The 5 keV FIB patterns showed a better IQ than the 30 keV FIB surfaces for each SEM accelerating voltage. The IQ of the EBSPs obtained using the 30 kV SEM accelerating voltage were higher than either of the patterns obtained at 20 kV. These results are consistent with the theory that lower ion beam energies induce less amorphization damage. Thus, higher quality diffraction patterns are expected for Si with less amorphization thickness, because absorption of the backscattered electrons would be less with a thinner amorphous layer. In addition, the patterns obtained at an SEM accelerating voltage of 30 kV were of higher quality than the patterns obtained at the 20 kV, because the ratio of the electron interaction volume to amorphous layer increases. It should be noted that, despite the range of IQ in the patterns, the patterns were consistently indexed for all of the images in Fig. 5. The best IQ of Si surfaces may be obtained using a combination of a low FIB beam energy with a high SEM accelerating voltage; however, suitable EBSPs may be obtained with other combinations of FIB energy and SEM accelerating voltage.

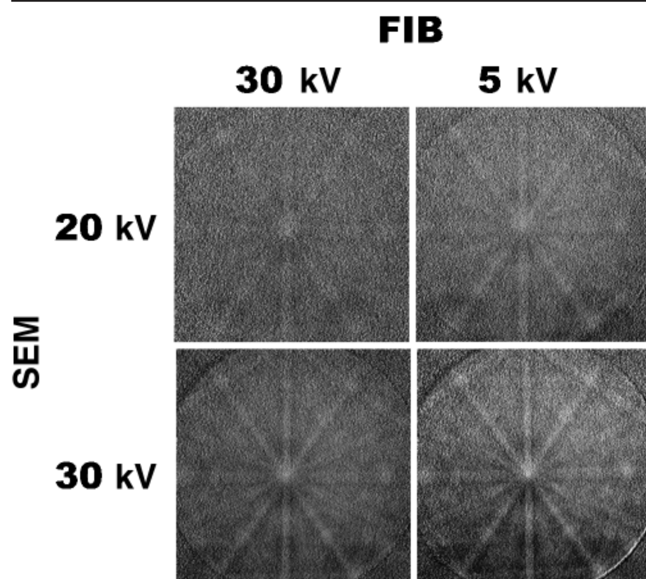

Fig. 5. The EBSPs from Si: a 30 keV Ga^+ FIB cut obtained with an SEM accelerating voltage of 20 kV, a 5 keV Ga^+ FIB cut obtained with an SEM accelerating voltage of 20 kV, a 30 keV Ga^+ FIB cut obtained with an SEM accelerating voltage of 30 kV, and a 5 keV Ga^+ FIB cut obtained with an SEM accelerating voltage of 30 kV.

Comparison of Cu and Si EBSD Results

Using a Monte Carlo simulation called TRIM,[16] the projected Ga^+ ion range, R_p, may be predicted for both Cu and Si at the ion beam energies and incident angles used in this study. The ion range may be represented schematically by the diagrams in Fig. 6. These R_p values for Cu and Si are summarized in Table I. It is noted that TRIM assumes that the target is amorphous. In addition, ion channeling in Cu can significantly reduce the sputtering yield and, hence, increase the R_p value.[17] Nevertheless, TRIM is an excellent tool for comparing ion interaction trends. Note that the R_p value for the 5 keV Si is less than the R_p value for the 30 keV Cu (e.g., 2.4 nm versus 3.8 nm). Using the Bethe approximation given in Ref. 18, for an electron energy of 20 keV, an electron range for Si and Cu (or the EBSD information depth) may be determined at an electron loss of 100 eV and a 70° incident angle. Table I shows that the EBSD information depth for Si is greater than for Cu at 20 kV (e.g., 28.2 nm versus 9.2 nm). Hence, one would expect that the EBSP of the 5 keV Ga^+ Si obtained with a 20 kV electron beam would be of higher quality than the 30 keV Ga^+ Cu. However, the Cu does not amorphize when bombarded with Ga^+, but Si does. Therefore, the FIB amorphization damage absorbs some of the backscattered electrons that degrade the EBSPs. The Cu surface remains crystalline during FIB milling (albeit with a Ga^+ implanted region) and, thus, EBSPs are readily obtainable from the FIB prepared Cu surface.

In the cases observed in this study, the electron interaction volume for BSEs is always greater than the R_p for Ga^+. The stopping power for electron scales with the stopping power for Ga^+ ions. The R_p for Ga^+ is three times less than the electron interaction necessary to acquire an EBSP for electron energies in the 5 keV to 30 keV range at these incident angles. Thus, it appears that EBSD analysis of many crystalline materials FIB milled by 30 keV Ga^+ (depending on ion incident angle) should be achievable. The FIB milling at lower beam energies will yield even better EBSD results.

The Application of EBSD to Dual Beam Instrumentation

Dual beam instruments that have an electron column and an ion column on the same platform allow the flexibility of cutting with the ion beam and imaging with either beam.[19] In addition, compositional analysis is also available on these instruments via SIMS and/or energy dispersive spectroscopy (EDS). Computer scripted algorithms enable FIB milling and SEM imaging to be performed automatically. It is envisioned that three-dimensional crystallographic orientation analysis of materials could also be incorporated into a dual beam via EBSD analysis. The combination of an ion beam, electron beam, SIMS, EDS, and EBSD would allow for site-specific three-dimensional crystallographic analysis of mul-

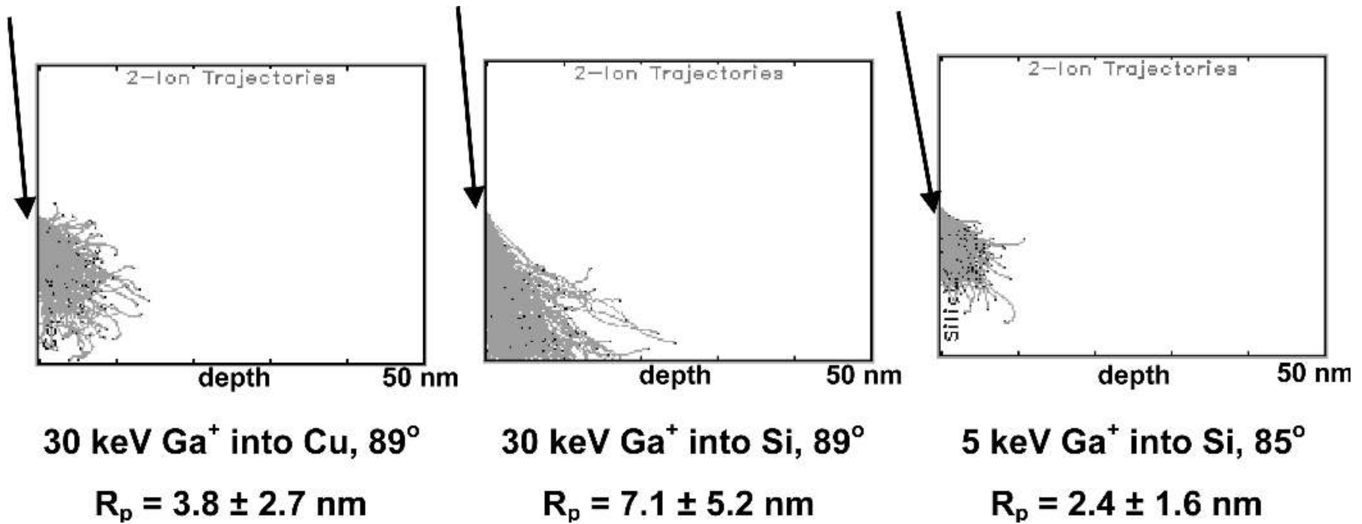

Fig. 6. The TRIM simulations for the Cu and Si experimental conditions as described in the text.

Table I. Comparison of Ion Damage Depth with EBSP Information Limit

Material	Ga^+ R_p Values (nm) 89° and 30 keV	Ga^+ R_p Values (nm) 85° and 5 keV	EBSP Surface Limit 20kV/70° (nm)
Cu	3.8 ± 2.7*	—	9.2
Si	7.1 ± 5.2*	2.4 ± 1.6*	28.2

tiphase and polycrystalline materials. In addition, the use of the channeling contrast obtained via ion imaging (or electron imaging) may be used to make EBSD analysis faster. For example, the EBSD could be automated to obtain diffraction patterns from only those regions where single grains are observed in the image. The number of collected patterns per unit area could vary depending on the size and variation of the observed channeling contrast in the image. That is, in regions where a large single crystal was observed, the number of patterns collected could be limited to just a few points. However, in regions where small, multiple, or unresolved grains or phases are observed, a larger density of patterns could be collected and analyzed. The addition of an EBSD detector to a dual beam instrument could significantly advance the understanding of microstructure, texture, and crystallographic relationships of grains and phases in three dimensions.

CONCLUSIONS

The FIB milled surfaces prepared in Si and Cu at a 20° stage tilt provided surfaces that were directly available for EBSD analysis in an SEM. The EBSPs that could automatically be indexed were successfully obtained for both the Si and the Cu despite the FIB damage that is unique to these materials. The EBSP image quality could be directly explained in terms of the electron interaction volume range compared with the FIB damage layer thickness. The successful application of EBSD analysis to FIB milled surfaces suggests that an EBSD detector incorporated into a dual beam instrument would be an enormously powerful technique.

ACKNOWLEDGEMENTS

The support of NSF DMR Grant No. 9703281 and the I4/UCF/Cirent Partnership is gratefully acknowledged. Helpful discussions with David Dingley and Brenda Prenitzer are greatly appreciated.

REFERENCES

1. David J. Dingley, *Electron Backscatter Diffraction in Materials Science,* ed. Adam J. Schwartz, Mukul Kumar, and Brent L. Adams (New York: Kluwer Academic/Plenum Publishers, 2000), pp. 1–16.
2. *OIM Analysis for Windows, User Manual* (TexSem Laboratories, Inc., Draper, UT, 1997), p. 5.
3. B.L. Adams, S.I. Wright, and K. Kunze, *Metall. Trans. A* 24A, 819 (1993).
4. Dale E. Newbury, David C. Joy, Patrick Echlin, Charles E. Fiori, and Joseph I. Goldstein, *Advanced Scanning Electron Microscopy and X-Ray Microanalysis* (New York: Plenum Press, 1986), p. 105.
5. D.J. Dingley, *Scanning Electron Microsc.* 4, 273 (1981).
6. C.J. Harland, P. Akhter, and J.A. Venables, *J. Phys. E* 14, 175 (1981).
7. F.A. Stevie, C.B. Vartuli, L.A. Giannuzzi, T.L. Shofner, S.R. Brown, B. Rossie, F. Hillion, R.H. Mills, M. Antonell, R.B. Irwin, and B.M. Purcell, *Surf. Interface Anal.* 31, 345 (2001).
8. M. Nastasi, J.W. Mayer, and J.K. Hirvonen, *Ion-Solid Interactions: Fundamentals and Applications* (New York: Cambridge University Press, 1996), pp. 354–355.
9. M. Nastasi, J.W. Mayer, and J.K. Hirvonen, *Ion-Solid Interactions: Fundamentals and Applications* (New York: Cambridge University Press, 1996) pp. 133–139.
10. David W. Susnitzky and Kevin D. Johnson, *Microsc. Microanal.* 4, 656 (1998).

11. C.A. Urbanik, B.I. Prenitzer, L.A. Giannuzzi, S.R. Brown, T.L. Shofner, B. Rossie, R.B. Irwin, and F.A. Stevie, *Microscopy & Microanalysis,* Proc.: Microscopy & Microanalysis 99, vol. 5 (Microscopy Society of America, 1999), pp. 740–741.
12. L.A. Giannuzzi and F.A. Stevie, *Microscopy & Microanalysis,* Proc.: Microscopy & Microanalysis 99, vol. 6, (Microscopy Society of America, 2000), pp. 508–509.
13. L.A. Giannuzzi, J.L. Drown, S.R. Brown, R.B. Irwin, and F.A. Stevie, *Workshop on Specimen Preparation for TEM of Materials IV,* vol. 480, (Pittsburgh, PA: Materials Research Society, 1997), pp. 19–27.
14. L.A. Giannuzzi, J.L. Drown, S.R. Brown, R.B. Irwin, F.A. Stevie, *Microsc. Res. Techn.* 41, 285 (1998).
15. L.M. Gignac, K.P. Rodbell, C. Murray, and M.J. Gribelyuk (Paper presented at ASM 2000, St. Louis, MO, 2000).
16. J.F. Ziegler, *Ion Beam Interactions With Matter: Introduction of SRIM,* http://www.research.ibm.com/ionbeams/home.htm#Home:SRIM Manual (1998).
17. B.W. Kempshall, S.M. Schwarz, B.I. Prenitzer, L.A. Giannuzzi, and F.A. Stevie, *J. Vac. Sci. Technol. B* 19, 749 (2001).
18. Joseph I. Goldstein, Dale E. Newbury, Patrick Echlin, David C. Joy, A.D. Romig, Jr., Charles E. Lyman, Charles Fiori, Charles, and Eric Lifshin, *Scanning Electron Microscopy and X-Ray Microanalysis,* 2nd ed. (New York: Plenum Press, 1992), pp. 76–89.
19. R.J. Young, *Microscopy & Microanalysis,* Proc.: Microscopy & Microanalysis 99, vol. 6, (Microscopy Society of America, 2000), pp. 512–513.